Monthly Notices
of the
ROYAL ASTRONOMICAL SOCIETY

MNRAS **493,** 2952–2964 (2020)
Advance Access publication 2020 February 11

doi:10.1093/mnras/staa335

# The GALAH survey: chemodynamics of the solar neighbourhood

Michael R. Hayden,[1,2]★ Joss Bland-Hawthorn,[1,2] Sanjib Sharma,[1,2] Ken Freeman,[3] Janez Kos,[1,4] Sven Buder,[5] Borja Anguiano,[6] Martin Asplund,[2,3] Boquan Chen,[1,2] Gayandhi M. De Silva,[1,7] Shourya Khanna,[1,2] Jane Lin,[3] Jonathan Horner,[8] Sarah Martell,[2,9] Yuan-Sen Ting,[10,11,12] Rosemary Wyse,[13] Daniel Zucker[7] and Tomaz Zwitter[4]

[1]*Sydney Institute for Astronomy, School of Physics, University of Sydney, NSW 2006, Australia*
[2]*ARC Centre of Excellence for All Sky Astrophysics in 3D (ASTRO-3D), Australia*
[3]*Research School of Astronomy & Astrophysics, Australian National University, ACT 2611, Australia*
[4]*Faculty of Mathematics and Physics, University of Ljubljana, Jadranska 19, 1000 Ljubljana, Slovenia*
[5]*Max Planck Institute for Astronomy (MPIA), Koenigstuhl 17, D-69117 Heidelberg, Germany*
[6]*Department of Astronomy, University of Virginia, Charlottesville, VA 22904, USA*
[7]*Department of Physics and Astronomy, Macquarie University, Sydney NSW 2109, Australia*
[8]*Centre for Astrophysics, University of Southern Queensland, Toowoomba Qld 4350, Australia*
[9]*School of Physics, University of New South Wales, Sydney NSW 2052, Australia*
[10]*Institute for Advanced Study, Princeton, NJ 08540, USA*
[11]*Department of Astrophysical Sciences, Princeton University, Princeton, NJ 08544, USA*
[12]*Observatories of the Carnegie Institution of Washington, 813 Santa Barbara Street, Pasadena, CA 91101, USA*
[13]*Department of Physics & Astronomy, Johns Hopkins University, Baltimore, MD 21218, USA*

Accepted 2020 January 13. Received 2020 January 6; in original form 2019 January 22

## ABSTRACT

We present the chemodynamic structure of the solar neighbourhood using 55 652 stars within a 500 pc volume around the Sun observed by GALAH and with astrometric parameters from *Gaia* DR2. We measure the velocity dispersion for all three components (vertical, radial, and tangential) and find that it varies smoothly with [Fe/H] and [$\alpha$/Fe] for each component. The vertical component is especially clean, with $\sigma_{v_z}$ increasing from a low of 10 km s$^{-1}$ at solar [$\alpha$/Fe] and [Fe/H] to a high of more than 50 km s$^{-1}$ for more metal-poor and [$\alpha$/Fe] enhanced populations. We find no evidence of a large decrease in the velocity dispersion of the highest [$\alpha$/Fe] populations as claimed in surveys prior to *Gaia* DR2. The eccentricity distribution for local stars varies most strongly as a function of [$\alpha$/Fe], where stars with [$\alpha$/Fe] $< 0.1$ dex having generally circular orbits ($e < 0.15$), while the median eccentricity increases rapidly for more [$\alpha$/Fe] enhanced stellar populations up to $e \sim 0.35$. These [$\alpha$/Fe] enhanced populations have guiding radii consistent with origins in the inner Galaxy. Of the stars with metallicities much higher than the local interstellar medium ([Fe/H] $> 0.1$ dex), we find that the majority have $e < 0.2$ and are likely observed in the solar neighbourhood through churning/migration rather than blurring effects, as the epicyclic motion for these stars is not large enough to reach the radii at which they were likely born based on their metallicity.

**Key words:** Galaxy: abundances – Galaxy: kinematics and dynamics – Galaxy: stellar content – Galaxy: structure.

## 1 INTRODUCTION

Galactic archaeology is the study of the structure and history of the Milky Way with the aim of understanding galaxy evolution using the fully resolved stellar inventory, from the long-lived, low-mass dwarfs to the most massive, hot young stars (Freeman & Bland-Hawthorn 2002). The Milky Way provides a unique test bed for many theories of galaxy evolution due to the ability to resolve individual stars and stellar populations, which is generally not possible in external galaxies. Stars contain the chemical fingerprint of the gas from which they formed, and can be used as fossil records to look back in time and see how the interstellar medium (ISM) of the Galaxy has evolved. Despite this, there is much debate about the

★ E-mail: michael.hayden@sydney.edu.au

© 2020 The Author(s)
Published by Oxford University Press on behalf of the Royal Astronomical Society

Downloaded from https://academic.oup.com/mnras/article/493/2/2952/5733167 by piyush.suneet@gmail.com on 24 July 2021

different structural properties of the Galaxy as a whole (e.g. Rix & Bovy 2013; Bland-Hawthorn & Gerhard 2016). The primary cause of that debate is the poor observational constraints on the various models, which is a problem even for the solar neighbourhood.

The chemodynamic structure of the solar neighbourhood is a complex mesh of many different stellar populations that have been built up over the history of the Milky Way. The stars that are found close to the Sun today span a huge range in age and come from a variety of birth radii. This is most easily demonstrated by the large number of supersolar metallicity ([Fe/H] $>$ 0.1 dex) stars observed in the solar neighbourhood and lack of an overall age–metallicity relationship (e.g. Casagrande et al. 2011; Haywood et al. 2013; Bergemann et al. 2014; Kordopatis et al. 2015; Buder et al. 2019; Hayden et al. 2018). Stars with [Fe/H] $>$ 0.1 dex are too metal rich to have formed in the solar neighbourhood as the local ISM metallicity today is well established from the B star population at slightly subsolar values (Nieva & Przybilla 2012). The likely origin of these stars is the inner Galaxy, as there are strong radial metallicity gradients in the disc where the median metallicity of stars in the inner Galaxy is much higher than in the solar neighbourhood (e.g. Luck & Lambert 2011; Lemasle et al. 2013; Anders et al. 2014; Hayden et al. 2014).

The local ISM appears to be fairly well mixed, with young population tracers such as B stars and Cepheids showing only small-scale variation over a large range in azimuth (Luck et al. 2011; Nieva & Przybilla 2012, but see also Balser et al. 2011, 2015 that do find variations in H II regions with azimuth). How supersolar metallicity stars reach the solar neighbourhood is an open question. Radial mixing processes have been proposed to explain the chemodynamic properties of the Galaxy (e.g. Sellwood & Binney 2002; Schönrich & Binney 2009; Minchev & Famaey 2010), which are differentiated by the effect on the angular momentum of the orbits. In blurring, stellar orbits become heated with time and have large epicyclic motions over their orbit, but the angular momentum remains conserved. In churning (migration), there is a change in angular momentum of an orbit due to interactions associated with non-axisymmetric structure (i.e. spiral arms or the bar). Changing the angular momentum of an orbit causes a change in guiding radius, and if the interaction is due to a co-rotation resonance, other parameters such as eccentricity are preserved. Stars are equally likely to migrate in or out. If spiral arms are transient, the net effect is to move stars to larger radii due to the exponential density law of the stellar disc.

The velocity dispersions of stellar populations in the solar neighbourhood contain potential hints of a major merger early on in the history of the Galaxy (Minchev et al. 2014). The velocity dispersion is generally observed to increase with age, as older populations get heated with time or were potentially born in a kinematically hotter environment than the present star-forming disc, which has a scale height of $<$100 pc (Bland-Hawthorn & Gerhard 2016). However, observations using data from RAVE have shown a downturn in the velocity dispersion for the highest [$\alpha$/Fe] (i.e. likely the oldest) stellar populations across a range of metallicities in the solar neighbourhood (Minchev et al. 2014). This same signature was observed in the simulations of Minchev, Chiappini & Martig (2013), who found that a major merger at $z \sim 2$ drove enhanced radial migration of stellar populations to the solar neighbourhood. Migration can cool the disc as stars that migrate often have cooler kinematics than stars of the same age that are born locally (e.g. Minchev et al. 2012; Vera-Ciro et al. 2014). This result was less obvious in observations from the *Gaia*-ESO survey (Guiglion et al. 2015; Hayden et al. 2018), which showed a shallower turnover in the velocity dispersion for higher [$\alpha$/Fe] populations compared to the RAVE results.

Our present understanding of the Milky Way is in the midst of a revolution. With the advent of large-scale spectroscopic surveys such as SEGUE (Yanny et al. 2009), RAVE (Steinmetz et al. 2006), LAMOST (Deng et al. 2012), APOGEE (Majewski et al. 2017), GALAH (De Silva et al. 2015), and future surveys such as 4MOST (de Jong et al. 2014) and WEAVE (Dalton et al. 2014), spectroscopic observations will be available for millions of stars in all Galactic components. Combined with the addition of precise astrometric information from the *Gaia* satellite (Perryman et al. 2001), we will have the ability to determine the precise kinematic, dynamic, and temporal structure of stellar populations throughout the Galaxy. *Gaia* alone has found an incredible amount of substructure in velocity and action space in the solar neighbourhood (e.g. Antoja et al. 2018; Trick, Coronado & Rix 2018). The precise kinematic properties estimated by *Gaia* used in conjunction with detailed chemistry estimates from the large spectroscopic surveys mentioned above provide the best picture to date of the structure and evolution of the Milky Way.

For this paper, we use observations of tens of thousands of stars found within 500 pc of the solar position from GALAH DR2 (Buder et al. 2018) and astrometric information from *Gaia* DR2 (Gaia Collaboration et al. 2018) to unravel the structure of the local disc. GALAH is a high-resolution ($R \sim 28\,000$) spectroscopic survey of nearly one million stars throughout the Milky Way, which provides precise atmospheric parameters and abundances for dozens of elements. Used in conjunction with proper motions and parallax measurements from *Gaia* DR2, we are able estimate orbital properties for the entire GALAH solar neighbourhood sample to map out the chemodynamic structure of the local disc. This paper is organised as follows. In Section 2, we discuss the data used in our analysis. In Section 3, we present our results on the velocity dispersion and orbital properties as a function of chemistry for stars near the solar position, and in Section 4, we discuss our findings in the context of the chemodynamic structure of the solar neighbourhood, before drawing our conclusions in Section 5.

## 2 DATA

Spectroscopic data are taken from the internal GALAH DR2 release, which contains the public DR2 (Buder et al. 2018), and also additional fields for K2 (Wittenmyer et al. 2018) and TESS (Sharma et al. 2018) follow-up that contain large numbers of stars in the solar neighbourhood. GALAH uses the High Efficiency and Resolution Multi-Element Spectrograph (HERMES; Sheinis et al. 2015) instrument, which is a high resolution ($R \sim 28000$) multifibre spectrograph mounted on the 3.9 m Anglo Australian Telescope (AAT). HERMES covers four wavelength ranges (4713–4903, 5648–5873, 6478–6737, and 7585–7887Å), carefully selected to maximize the number of elemental abundances that are able to be measured. Observations are reduced through a standardized pipeline developed for the GALAH survey as described in Kos et al. (2017). Stellar atmospheric parameters and individual abundances are derived using a combination of SME (Valenti & Piskunov 1996; Piskunov & Valenti 2017) to develop a large training set covering parameter space, which is then fed into the Cannon (Ness et al. 2015) to obtain estimates for the entire sample. The precision of individual abundances [X/Fe] is typically $\sim$0.05 dex, while the random errors in radial velocities are $\sim$100 m s$^{-1}$ (Zwitter et al. 2018). For [$\alpha$/Fe], we use an average of the Ti, Mg, and Al abundances from GALAH DR2. Data quality cuts are listed in Table 1. As we are interested

Downloaded from https://academic.oup.com/mnras/article/493/2/2952/5733167 by piyush.suneet@gmail.com on 24 July 2021

**Table 1.** Data cuts used on the GALAH DR2 *Gaia* DR2 sample.

| Flag | Value |
|---|---|
| cannon_flag[1] | 0 |
| abundance_flag[1] | <3 |
| SNR | >20 |
| $\sigma_{T_{eff}}$ | <200 K |
| [Fe/H] | $-1.0 <$ [Fe/H] $< 0.5$ dex |
| $d_s$ | <500 pc |
| RUWE (*Gaia*) | <1.4 |

*Note.* A description of the data flag bitmasks can be found here: https://datacentral.org.au/docs/pages/galah/table-schema/dr2-table-schema/.

primarily in the chemodynamics of the disc, we restrict our sample to $-1.0 <$ [Fe/H] $< 0.5$ dex in an attempt to minimize the impact of the halo in our analysis, in particular estimates of the velocity dispersion.

Astrometric parameters are taken from *Gaia* DR2 (Gaia Collaboration et al. 2018), which have random errors on the order of a few per cent for the local sample used in this paper. We restrict our sample to stars within 500 pc, with the aim of studying the stellar populations of the local volume. This sample contains 55 652 stars that span a range of stellar parameters and metallicities, as shown in Fig. 1. The local volume is dominated by dwarf stars. In order to test the impact of the GALAH selection function on the metallicity distribution function(MDF), we generated mock stellar samples of the Galaxy with *Galaxia* (Sharma et al. 2011), one sampling all visible stars within 500 pc to generate an intrinsic MDF of the solar neighbourhood, and another imposing the GALAH lines of sight and magnitude distributions. We then compared the intrinsic MDF (orange curve) to the MDF with the GALAH selection function imposed (green curve) and found no difference in metallicity between the samples, as shown in Fig. 2.

An interesting feature of the MDF, here measured using the iron abundance relative to solar values [Fe/H] (Asplund et al. 2009), is that 45 per cent of stars in the sample are solar metallicity or above, and 25 per cent have metallicities >0.1 dex. The distribution of stars in the [$\alpha$/Fe] versus [Fe/H] plane, showing the clear separation between the chemical thick and thin discs at lower metallicities, is shown in Fig. 3. The grey lines denote the different metallicity and [$\alpha$/Fe] bins used in our analysis. With the exception of the lowest [$\alpha$/Fe] bin, the sample is divided in [$\alpha$/Fe] at fixed increments of 0.08 dex and the zero-points chosen such that the overlap between the chemical thick and thin discs is minimized. The lowest [$\alpha$/Fe] bin has a width of 0.12 dex. The metallicity bins are spaced by 0.2 dex, with the exception of the most metal-rich and metal-poor bins.

### 2.1 Distances and Orbits

The distances to stars are derived using the estimated parallax from *Gaia* DR2 and a Bayesian technique similar to that outlined in Bailer-Jones (2015). We assume a simple prior with a single exponential disc that has a scale height of 300 pc and a scale length of 2.7 kpc, which is used to generate a probability distribution (PDF) in distance space. The distance is characterized by the mode of the PDF, while the errors in distance are estimated using the 16th and 84th percentiles of the PDF. As the sample is restricted to stars within 500 pc of the Sun, the parallax accuracy is high (<10 per cent error). However, not all parallax measurements, even those with small fractional errors, are reliable due to various issues. Therefore, we additionally require that the renormalized unit weight error (RUWE) < 1.4, ensuring we only use stars for which the estimated parallaxes are robust.

Kinematic and orbital properties for each star are derived with *Galpy* (Bovy 2015) using the Stäckel analytic approximations outlined in Mackereth & Bovy (2018) and the default 'MWHaloPotential2014', rescaled such that $R_\odot = 8.2$ kpc and the local circular velocity is 238 km s$^{-1}$ (Bland-Hawthorn & Gerhard 2016). The solar motion relative to the local standard of rest (LSR) of $(U_\odot,V_\odot,W_\odot) = (11.65, 12.24, 7.25)$ is used (Schönrich, Binney & Dehnen 2010). Eccentricities are estimated using *Galpy*, and are

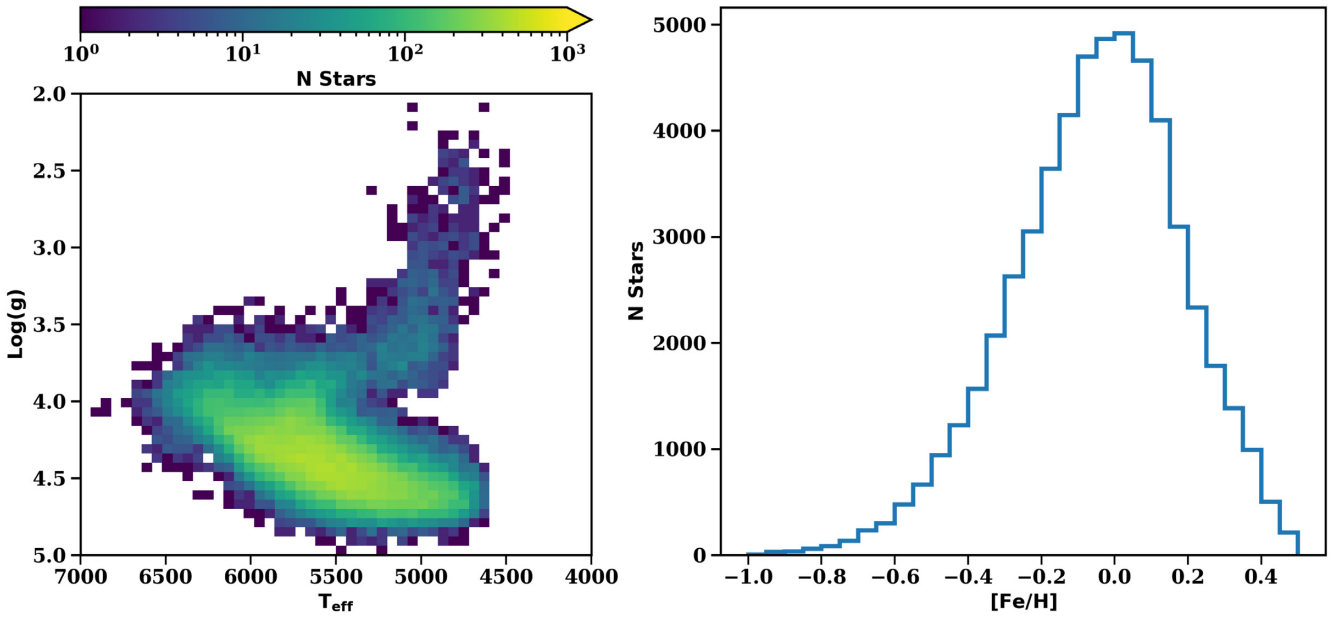


**Figure 1.** Left: The H–R diagram for our sample of 62 814 GALAH stars within 500 pc of the solar position. Right: The MDF of the sample. Note the large fraction of supersolar metallicities stars despite the local ISM being ∼solar metallicity.

Downloaded from https://academic.oup.com/mnras/article/493/2/2952/5733167 by piyush.suneet@gmail.com on 24 July 2021

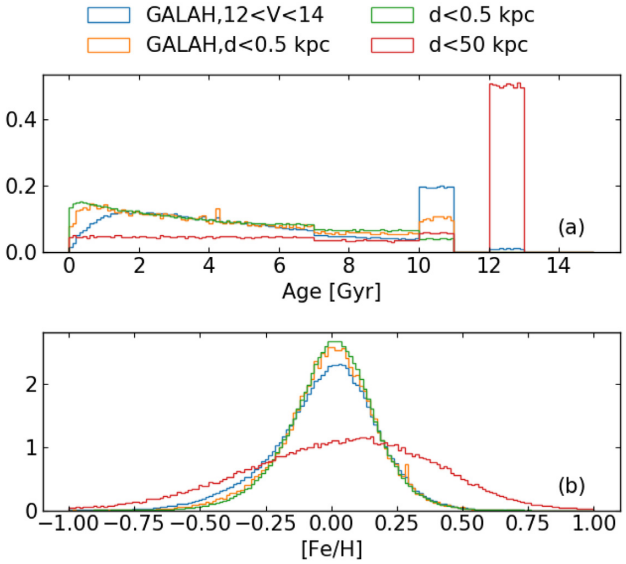


**Figure 2.** A *Galaxia* representation of the stellar populations of the Milky Way (red) and in the solar neighbourhood (orange), with the impact of the GALAH selection function for the entire Galaxy (blue) and in the solar neighbourhood (orange) on the observed stellar populations. (a) The impact of the GALAH selection function on the age distribution of stars observed in the solar neighbourhood (green) relative to the underlying distribution of stars in the solar neighbourhood in *Galaxia* (orange). The GALAH selection function has a minimal impact on the observed age distribution. (b) The impact of the GALAH selection function on the observed MDF of the solar neighbourhood compared to underlying MDF in the model (orange). The observed MDF is unaffected by the GALAH lines of site and magnitude limits compared to the underlying population.

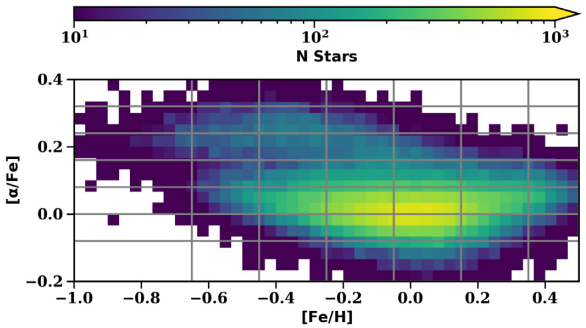


**Figure 3.** The [$\alpha$/Fe] versus [Fe/H] plane for the GALAH sample within 500 pc of the solar position. Grey lines denote the bins in metallicity and [$\alpha$/Fe] used later in this paper.

defined as

$$e = \frac{R_{\rm ap} - R_{\rm peri}}{R_{\rm ap} + R_{\rm peri}}, \tag{1}$$

where $R_{\rm ap}$ is the apogalacticon of the orbit, and $R_{\rm peri}$ is the perigalacticon of the orbit.

1000 MC runs of each orbit are performed using the errors in distance, radial velocity, and proper motion to estimate the uncertainties in each orbital parameter. Typical uncertainties in the individual velocity components are $<1$ km s$^{-1}$, as shown in Fig. 4. It is important to stress that this is more than an order of magnitude improvement in the velocity determination compared to previous studies analysing the velocity distributions of the solar neighbourhood (e.g. Minchev et al. 2014; Guiglion et al. 2015; Hayden et al. 2018). This is due to a combination of precise radial velocities from GALAH DR2, which have an accuracy of 0.1–0.2 km s$^{-1}$ (Zwitter et al. 2018), and the dramatic improvement in proper motions and parallaxes from *Gaia* DR2. Velocity dispersions are measured using the equations outlined below for each [$\alpha$/Fe] and [Fe/H] bin, which take into account the errors in individual velocity measurements when computing the dispersion:

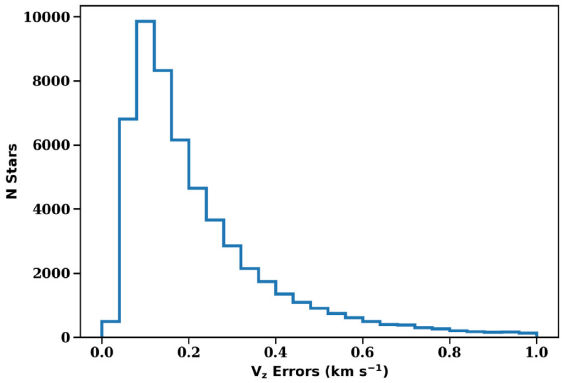


**Figure 4.** The distribution of errors in the vertical velocity component. Errors in the radial and tangential components are comparable to those in the vertical component. Velocities are determined with proper motions from *Gaia* DR2 and radial velocities from GALAH DR2, while errors are estimated via 1000 Monte Carlo runs from the input parameters and their uncertainties. The errors in this sample for the individual velocity components are an order of magnitude improvement over previous studies.

$$L(\mu, \sigma_i) = \prod_{i=1}^{N} \frac{1}{\sqrt{2\pi\left(\sigma_i^2 + ev_i^2\right)}} \exp\left(-\frac{1}{2}\frac{(v_i - \mu)^2}{\left(\sigma_i^2 + ev_i^2\right)}\right), \tag{2}$$

where $\sigma_i$ is the velocity dispersion, $\mu$ is the average velocity, $v_i$ is the velocity of a given star, and $ev_i$ is the error in the velocity. We minimize the log-likelihood $\Lambda \equiv 2\ln L$ by solving where the partial derivatives of $\Lambda$ are zero, i.e. $\frac{\partial\Lambda}{\partial\mu}$ and $\frac{\partial\Lambda}{\partial\sigma_i}$, which gives

$$\sum_{i=1}^{N} \frac{v_i}{\left(\sigma_i^2 + ev_i^2\right)} - \mu \sum_{i=1}^{N} \frac{1}{\sigma_i^2 + ev_i^2} = 0 \tag{3}$$

$$\sum_{i=1}^{N} \frac{\left(\sigma_i^2 + ev_i^2\right)^2 - (v_i - \mu)^2}{\left(\sigma_i^2 + ev_i^2\right)^2} = 0 \tag{4}$$

(see also Godwin & Lynden-Bell 1987; Pryor & Meylan 1993). As the velocity dispersion is sensitive to extreme outliers, we remove stars more than three standard deviations away from the median in any given bin. Errors in the velocity dispersion are estimated using 10 000 bootstrap runs of the sample in each given bin. We also note that the $\sigma_{v_\phi}$ may be underestimated due to the velocity distributions being asymmetric and non-Gaussian. Tian et al. (2015) found that $\sigma_{v_\phi}$ could systematically underestimated in high dispersion populations because of this non-Gaussianity.

## 3 RESULTS

The velocity dispersion is measured in bins of [$\alpha$/Fe] and [Fe/H] (see Fig. 3) for all three components, as shown in Fig. 5 and Table 2. There is a minimum of 20 stars per bin. We find that the vertical velocity dispersion (left-hand panel) increases smoothly with both [Fe/H] and [$\alpha$/Fe], in fact only for the most metal-rich stellar populations does one metallicity bin intersect another for the same [$\alpha$/Fe]. For stellar populations with the same [Fe/H], the

Downloaded from https://academic.oup.com/mnras/article/493/2/2952/5733167 by piyush.suneet@gmail.com on 24 July 2021

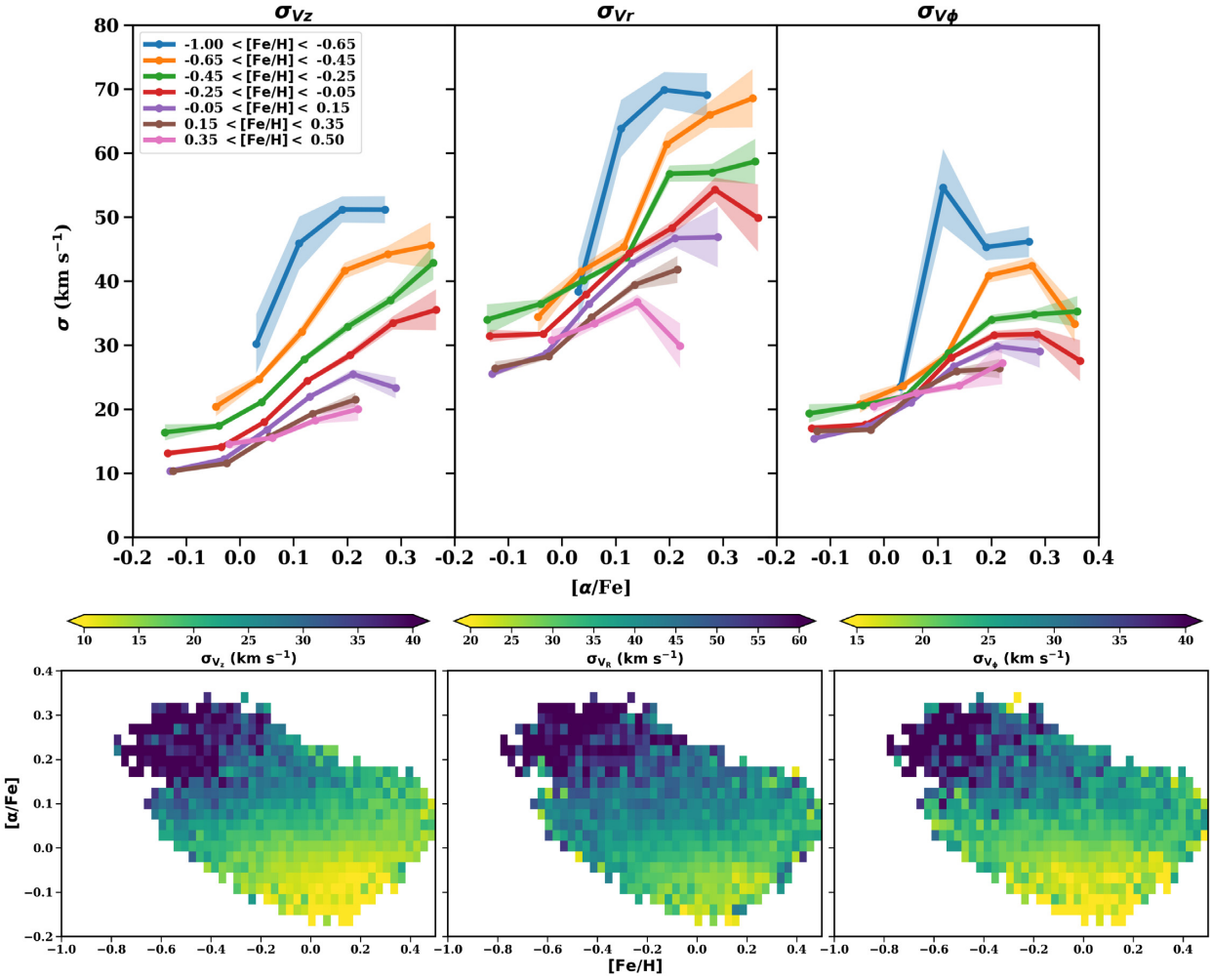


**Figure 5.** Top: The velocity dispersion as a function of [$\alpha$/Fe] and [Fe/H] for the GALAH solar neighbourhood sample. One-$\sigma$ errors are shown by the shaded lines. There is a minimum of 20 stars per bin. Bottom: Similar to above, but visualized in the [$\alpha$/Fe] versus [Fe/H] plane. There is a minimum of 10 stars per bin. The velocity dispersion varies smoothly with [$\alpha$/Fe] and [Fe/H], increasing with increasing [$\alpha$/Fe] or decreasing [Fe/H]. The colourbar limits are set to maximize contrast in each figure, there are some bins with velocity dispersions above (below) the upper (lower) limits in each panel.

velocity dispersion increases as [$\alpha$/Fe] increases. For populations with the same [$\alpha$/Fe], the velocity dispersion increases as [Fe/H] decreases. The overall range of the vertical velocity dispersion varies from 10 km s$^{-1}$ for the more metal-rich and subsolar [$\alpha$/Fe] abundances, to $\sim$50 km s$^{-1}$ for the most metal-poor [$\alpha$/Fe]-enhanced populations. There is also a change in behaviour of the velocity dispersion at a given [$\alpha$/Fe] as a function of metallicity at [$\alpha$/Fe]$\sim$0.1. For low-[$\alpha$/Fe] populations, the difference in velocity dispersion between metal-rich and metal-poor stars at a given [$\alpha$/Fe] is small, $<$10 km s$^{-1}$ in $\sigma_{v_z}$. At higher [$\alpha$/Fe] the dispersion has a much larger spread as a function of [Fe/H] at a given [$\alpha$/Fe], more than 30 km s$^{-1}$ in $\sigma_{v_z}$ for the highest [$\alpha$/Fe] populations. The radial (middle panel) and tangential (right-hand panel) velocity dispersion components follow these same trends, although with more overlap between stellar populations. The velocity dispersion is largest in the radial direction, increasing from $\sim$25 to $\sim$70 km s$^{-1}$, as [$\alpha$/Fe] increases and [Fe/H] decreases. The tangential velocity dispersion is generally small, with $V_\phi < 20$ km s$^{-1}$ for all but the most metal-poor stars with [$\alpha$/Fe] $< 0.1$ dex. In all components, we see a gradual flattening of the increase in velocity dispersion with increasing [$\alpha$/Fe] for the highest [$\alpha$/Fe] stellar populations. However, we find no evidence of dramatic decrease in velocity dispersion for these high-[$\alpha$/Fe] stellar populations.

The ratio of the vertical and rotational velocity dispersions to the radial velocity dispersion can give insight into the various heating mechanisms that affect the different stellar populations of the disc. The ratio of $\sigma_{v_z}/\sigma_{v_R}$ and $\sigma_{v_\phi}/\sigma_{v_R}$ is shown in Fig. 6 as a function of [Fe/H] and [$\alpha$/Fe]. $\sigma_{v_z}/\sigma_{v_R}$ strongly varies for different stellar populations. The lowest [$\alpha$/Fe] populations (chemical thin disc) have a ratio of $\sim$0.4, which gradually increases as [$\alpha$/Fe] increases, to $\sim$0.7 for the higher [$\alpha$/Fe] populations (chemical thick disk), and even reaches 0.8 for the most metal-poor stars. There is a slight metallicity dependence, with the more metal-poor populations in general having a higher ratio of $\sigma_{v_z}/\sigma_{v_R}$, with the exception of the most metal-rich bin ([Fe/H] $> 0.35$). However, this variation is less smooth than the trends identified in the individual velocity components themselves and certainly of much lower importance than the trend of increasing $\sigma_{v_z}/\sigma_{v_R}$ with [$\alpha$/Fe]. In contrast, the $\sigma_{v_\phi}/\sigma_{v_R}$ ratio shows no trend with metallicity or [$\alpha$/Fe], and is roughly constant within the errors for all stellar populations at $\sim$0.6.



Downloaded from https://academic.oup.com/mnras/article/493/2/2952/5733167 by piyush.suneet@gmail.com on 24 July 2021

**Table 2.** The chemodynamics of the solar neighbourhood for the GALAH sample.

| [α/Fe] range | [Fe/H] range | $N$ | $\widetilde{V}_\phi$ (km s$^{-1}$) | $\sigma v_z$ (km s$^{-1}$) | $\sigma_{v_r}$ (km s$^{-1}$) | $\sigma_{v_\phi}$ (km s$^{-1}$) | $\frac{\sigma_{v_z}}{\sigma_{v_r}}$ | $\frac{\sigma_{v_\phi}}{\sigma_{v_r}}$ | $\frac{\sigma_{v_z}}{\sigma_{v_\phi}}$ |
|---|---|---|---|---|---|---|---|---|---|
| −0.2 < [α/Fe] < −0.08 | −0.45 < [Fe/H] < −0.25 | 79 | 243.7 ± 2.8 | 16.4 ± 1.2 | 34.0 ± 2.4 | 19.3 ± 1.4 | 0.48 ± 0.05 | 0.57 ± 0.06 | 0.85 ± 0.09 |
| −0.2 < [α/Fe] < −0.08 | −0.25 < [Fe/H] < −0.05 | 464 | 240.2 ± 1.1 | 13.1 ± 0.4 | 31.4 ± 1.0 | 17.0 ± 0.5 | 0.42 ± 0.02 | 0.54 ± 0.02 | 0.77 ± 0.04 |
| −0.2 < [α/Fe] < −0.08 | −0.05 < [Fe/H] < 0.15 | 996 | 237.9 ± 0.6 | 10.4 ± 0.2 | 25.5 ± 0.6 | 15.4 ± 0.3 | 0.41 ± 0.01 | 0.6 ± 0.02 | 0.67 ± 0.02 |
| −0.2 < [α/Fe] < −0.08 | 0.15 < [Fe/H] < 0.35 | 322 | 232.4 ± 0.6 | 10.3 ± 0.4 | 26.4 ± 1.0 | 16.6 ± 0.7 | 0.39 ± 0.02 | 0.63 ± 0.04 | 0.62 ± 0.04 |
| −0.08 < [α/Fe] < 0.0 | −0.65 < [Fe/H] < −0.45 | 89 | 247.9 ± 2.3 | 20.4 ± 1.5 | 34.4 ± 2.5 | 20.8 ± 1.4 | 0.59 ± 0.06 | 0.61 ± 0.06 | 0.98 ± 0.1 |
| −0.08 < [α/Fe] < 0.0 | −0.45 < [Fe/H] < −0.25 | 1142 | 241.1 ± 0.8 | 17.4 ± 0.3 | 36.4 ± 0.7 | 20.6 ± 0.4 | 0.48 ± 0.01 | 0.57 ± 0.01 | 0.84 ± 0.02 |
| −0.08 < [α/Fe] < 0.0 | −0.25 < [Fe/H] < −0.05 | 4905 | 238.5 ± 0.3 | 14.1 ± 0.1 | 31.7 ± 0.3 | 17.6 ± 0.2 | 0.44 ± 0.01 | 0.55 ± 0.01 | 0.8 ± 0.01 |
| −0.08 < [α/Fe] < 0.0 | −0.05 < [Fe/H] < 0.15 | 6778 | 236.8 ± 0.3 | 12.2 ± 0.1 | 28.7 ± 0.2 | 17.3 ± 0.1 | 0.42 ± 0.01 | 0.6 ± 0.01 | 0.7 ± 0.01 |
| −0.08 < [α/Fe] < 0.0 | 0.15 < [Fe/H] < 0.35 | 2133 | 232.0 ± 0.3 | 11.5 ± 0.2 | 28.2 ± 0.4 | 16.8 ± 0.3 | 0.41 ± 0.01 | 0.59 ± 0.01 | 0.69 ± 0.02 |
| −0.08 < [α/Fe] < 0.0 | 0.35 < [Fe/H] < 0.5 | 166 | 227.9 ± 2.9 | 14.6 ± 0.8 | 30.8 ± 1.6 | 20.5 ± 1.1 | 0.47 ± 0.04 | 0.67 ± 0.05 | 0.71 ± 0.06 |
| 0.0 < [α/Fe] < 0.08 | −1.0 < [Fe/H] < −0.65 | 28 | 259.3 ± 5.0 | 30.2 ± 4.7 | 38.4 ± 5.1 | 23.5 ± 2.7 | 0.79 ± 0.16 | 0.61 ± 0.11 | 1.29 ± 0.25 |
| 0.0 < [α/Fe] < 0.08 | −0.65 < [Fe/H] < −0.45 | 747 | 242.2 ± 1.2 | 24.7 ± 0.6 | 41.5 ± 0.9 | 23.7 ± 0.5 | 0.6 ± 0.02 | 0.57 ± 0.02 | 1.04 ± 0.04 |
| 0.0 < [α/Fe] < 0.08 | −0.45 < [Fe/H] < −0.25 | 3311 | 239.4 ± 0.7 | 21.1 ± 0.3 | 40.1 ± 0.4 | 22.0 ± 0.3 | 0.53 ± 0.01 | 0.55 ± 0.01 | 0.96 ± 0.02 |
| 0.0 < [α/Fe] < 0.08 | −0.25 < [Fe/H] < −0.05 | 6844 | 236.3 ± 0.4 | 18.0 ± 0.2 | 37.9 ± 0.3 | 21.1 ± 0.2 | 0.47 ± 0.01 | 0.56 ± 0.01 | 0.85 ± 0.01 |
| 0.0 < [α/Fe] < 0.08 | −0.05 < [Fe/H] < 0.15 | 8055 | 231.8 ± 0.3 | 16.8 ± 0.1 | 36.4 ± 0.3 | 21.0 ± 0.2 | 0.46 ± 0.01 | 0.58 ± 0.01 | 0.8 ± 0.01 |
| 0.0 < [α/Fe] < 0.08 | 0.15 < [Fe/H] < 0.35 | 4520 | 226.4 ± 0.5 | 15.7 ± 0.2 | 34.3 ± 0.3 | 22.4 ± 0.2 | 0.46 ± 0.01 | 0.65 ± 0.01 | 0.7 ± 0.01 |
| 0.0 < [α/Fe] < 0.08 | 0.35 < [Fe/H] < 0.5 | 980 | 223.4 ± 1.2 | 15.5 ± 0.4 | 33.4 ± 0.8 | 22.5 ± 0.4 | 0.47 ± 0.01 | 0.67 ± 0.02 | 0.69 ± 0.02 |
| 0.08 < [α/Fe] < 0.16 | −1.0 < [Fe/H] < −0.65 | 59 | 214.2 ± 6.9 | 45.9 ± 4.2 | 63.8 ± 4.5 | 54.6 ± 6.0 | 0.72 ± 0.08 | 0.86 ± 0.11 | 0.84 ± 0.12 |
| 0.08 < [α/Fe] < 0.16 | −0.65 < [Fe/H] < −0.45 | 479 | 231.1 ± 1.6 | 32.1 ± 1.0 | 45.4 ± 1.4 | 28.2 ± 0.9 | 0.71 ± 0.03 | 0.62 ± 0.03 | 1.14 ± 0.05 |
| 0.08 < [α/Fe] < 0.16 | −0.45 < [Fe/H] < −0.25 | 1298 | 233.5 ± 1.2 | 27.8 ± 0.5 | 43.7 ± 0.8 | 28.8 ± 0.5 | 0.64 ± 0.02 | 0.66 ± 0.02 | 0.97 ± 0.03 |
| 0.08 < [α/Fe] < 0.16 | −0.25 < [Fe/H] < −0.05 | 1956 | 227.2 ± 0.8 | 24.4 ± 0.4 | 44.4 ± 0.6 | 28.0 ± 0.4 | 0.55 ± 0.01 | 0.63 ± 0.01 | 0.87 ± 0.02 |
| 0.08 < [α/Fe] < 0.16 | −0.05 < [Fe/H] < 0.15 | 1997 | 223.8 ± 1.0 | 21.9 ± 0.3 | 42.8 ± 0.6 | 26.7 ± 0.4 | 0.51 ± 0.01 | 0.62 ± 0.01 | 0.82 ± 0.02 |
| 0.08 < [α/Fe] < 0.16 | 0.15 < [Fe/H] < 0.35 | 1399 | 222.9 ± 0.9 | 19.3 ± 0.4 | 39.4 ± 0.7 | 25.9 ± 0.4 | 0.49 ± 0.01 | 0.66 ± 0.02 | 0.74 ± 0.02 |
| 0.08 < [α/Fe] < 0.16 | 0.35 < [Fe/H] < 0.5 | 490 | 224.0 ± 1.5 | 18.2 ± 0.5 | 36.7 ± 1.1 | 23.7 ± 0.6 | 0.5 ± 0.02 | 0.64 ± 0.03 | 0.77 ± 0.03 |
| 0.16 < [α/Fe] < 0.24 | −1.0 < [Fe/H] < −0.65 | 272 | 183.7 ± 2.1 | 51.2 ± 2.0 | 69.8 ± 2.9 | 45.3 ± 2.0 | 0.73 ± 0.04 | 0.65 ± 0.04 | 1.13 ± 0.07 |
| 0.16 < [α/Fe] < 0.24 | −0.65 < [Fe/H] < −0.45 | 515 | 197.7 ± 2.0 | 41.6 ± 1.2 | 61.4 ± 1.8 | 40.9 ± 1.1 | 0.68 ± 0.03 | 0.67 ± 0.03 | 1.02 ± 0.04 |
| 0.16 < [α/Fe] < 0.24 | −0.45 < [Fe/H] < −0.25 | 755 | 203.7 ± 1.6 | 32.8 ± 0.8 | 56.8 ± 1.3 | 34.0 ± 0.7 | 0.58 ± 0.02 | 0.6 ± 0.02 | 0.97 ± 0.03 |
| 0.16 < [α/Fe] < 0.24 | −0.25 < [Fe/H] < −0.05 | 863 | 206.6 ± 1.6 | 28.4 ± 0.7 | 48.3 ± 1.1 | 31.6 ± 0.7 | 0.59 ± 0.02 | 0.65 ± 0.02 | 0.9 ± 0.03 |
| 0.16 < [α/Fe] < 0.24 | −0.05 < [Fe/H] < 0.15 | 513 | 210.9 ± 1.8 | 25.5 ± 0.7 | 46.7 ± 1.3 | 29.8 ± 0.8 | 0.55 ± 0.02 | 0.64 ± 0.02 | 0.85 ± 0.03 |
| 0.16 < [α/Fe] < 0.24 | 0.15 < [Fe/H] < 0.35 | 144 | 210.5 ± 2.9 | 21.5 ± 1.1 | 41.8 ± 2.0 | 26.3 ± 1.5 | 0.51 ± 0.04 | 0.63 ± 0.05 | 0.82 ± 0.06 |
| 0.16 < [α/Fe] < 0.24 | 0.35 < [Fe/H] < 0.5 | 38 | 214.8 ± 6.5 | 20.0 ± 1.8 | 29.9 ± 3.5 | 27.2 ± 3.2 | 0.67 ± 0.1 | 0.91 ± 0.15 | 0.74 ± 0.11 |
| 0.24 < [α/Fe] < 0.32 | −1.0 < [Fe/H] < −0.65 | 182 | 171.6 ± 3.9 | 51.2 ± 2.2 | 69.1 ± 3.5 | 46.2 ± 2.3 | 0.74 ± 0.05 | 0.67 ± 0.05 | 1.11 ± 0.07 |
| 0.24 < [α/Fe] < 0.32 | −0.65 < [Fe/H] < −0.45 | 457 | 184.9 ± 2.3 | 44.2 ± 1.3 | 66.0 ± 2.1 | 42.4 ± 1.3 | 0.67 ± 0.03 | 0.64 ± 0.03 | 1.04 ± 0.04 |
| 0.24 < [α/Fe] < 0.32 | −0.45 < [Fe/H] < −0.25 | 748 | 196.6 ± 1.7 | 37.0 ± 0.9 | 56.9 ± 1.4 | 34.8 ± 0.8 | 0.65 ± 0.02 | 0.61 ± 0.02 | 1.06 ± 0.04 |
| 0.24 < [α/Fe] < 0.32 | −0.25 < [Fe/H] < −0.05 | 363 | 198.4 ± 2.5 | 33.5 ± 1.1 | 54.3 ± 1.9 | 31.7 ± 1.0 | 0.62 ± 0.03 | 0.58 ± 0.03 | 1.06 ± 0.05 |
| 0.24 < [α/Fe] < 0.32 | −0.05 < [Fe/H] < 0.15 | 44 | 201.7 ± 4.2 | 23.3 ± 1.6 | 46.9 ± 4.8 | 29.0 ± 2.5 | 0.5 ± 0.06 | 0.62 ± 0.08 | 0.8 ± 0.09 |
| 0.32 < [α/Fe] < 0.4 | −0.65 < [Fe/H] < −0.45 | 69 | 182.9 ± 4.4 | 45.6 ± 3.7 | 68.5 ± 4.5 | 33.3 ± 2.9 | 0.66 ± 0.07 | 0.49 ± 0.05 | 1.37 ± 0.16 |
| 0.32 < [α/Fe] < 0.4 | −0.45 < [Fe/H] < −0.25 | 111 | 188.7 ± 3.6 | 42.9 ± 2.6 | 58.7 ± 3.6 | 35.3 ± 2.4 | 0.73 ± 0.06 | 0.6 ± 0.05 | 1.22 ± 0.11 |
| 0.32 < [α/Fe] < 0.4 | −0.25 < [Fe/H] < −0.05 | 32 | 196.9 ± 5.7 | 35.5 ± 3.0 | 49.8 ± 5.5 | 27.6 ± 3.1 | 0.71 ± 0.1 | 0.55 ± 0.09 | 1.29 ± 0.18 |

We also measure the covariances of the velocity ellipsoid, which reflect the orientation of the velocity ellipsoid and are driven by non-axis symmetric structures in the Galactic potential. We characterize the deviation in the $R-\phi$ plane by the vertex deviation

$$l_v = \frac{1}{2}\arctan\left(\frac{2\sigma^2_{R\phi}}{\sigma^2_R - \sigma^2_\phi}\right) \quad (5)$$

and the $R-z$ plane by the tilt angle

$$\alpha = \frac{1}{2}\arctan\left(\frac{2\sigma^2_{Rz}}{\sigma^2_R - \sigma^2_z}\right). \quad (6)$$

We split our measurements first only by [α/Fe], and then only by [Fe/H], as shown in Fig. 7 and Table 3. There is too much noise to split into finer bins of both [Fe/H] and [α/Fe] as done with previous measurements in our analysis. We find that the tilt angle is roughly zero across the entire sample, with the exception of the highest [α/Fe] most metal-poor stellar populations, which have a slight tilt angle of 5 deg. The vertex deviation shows a gradual decline from 10 deg at the lowest [α/Fe] abundances to 5 deg for the highest [α/Fe] populations. As a function of [Fe/H], we see a similar trend where the vertex deviation increases from 5 deg for the most metal-poor stellar populations to ∼13 deg for the most metal-rich populations.

The distribution of rotational velocities as a function of chemistry shows several interesting trends, as shown in Fig. 8. For stars below [α/Fe] of ∼0.1–0.2 dex, metal-poor stars have larger rotational velocities than metal-rich stars with the same [α/Fe] abundance. However, the difference in rotational velocity between the difference stellar populations is not large, 25 km s$^{-1}$ for stars between $-0.65 <$ [Fe/H] $< 0.5$. However, these trends are reversed for higher [α/Fe] populations. For [α/Fe] $\gtrsim 0.2$, the more metal-rich stars have higher rotational velocities than the metal-poor stars with the same [α/Fe]. The rotational velocities for these stars are also much lower at higher [α/Fe] than for lower [α/Fe] stars at the same metallicity. The velocity difference between low-[α/Fe] and high-[α/Fe] populations is much greater than the velocity difference of different metallicity populations at the same [α/Fe].

Not all stars observed in the solar neighbourhood were born locally, and the origins of different stellar populations observed near the Solar position is an open question. The orbital properties

Downloaded from https://academic.oup.com/mnras/article/493/2/2952/5733167 by piyush.suneet@gmail.com on 24 July 2021

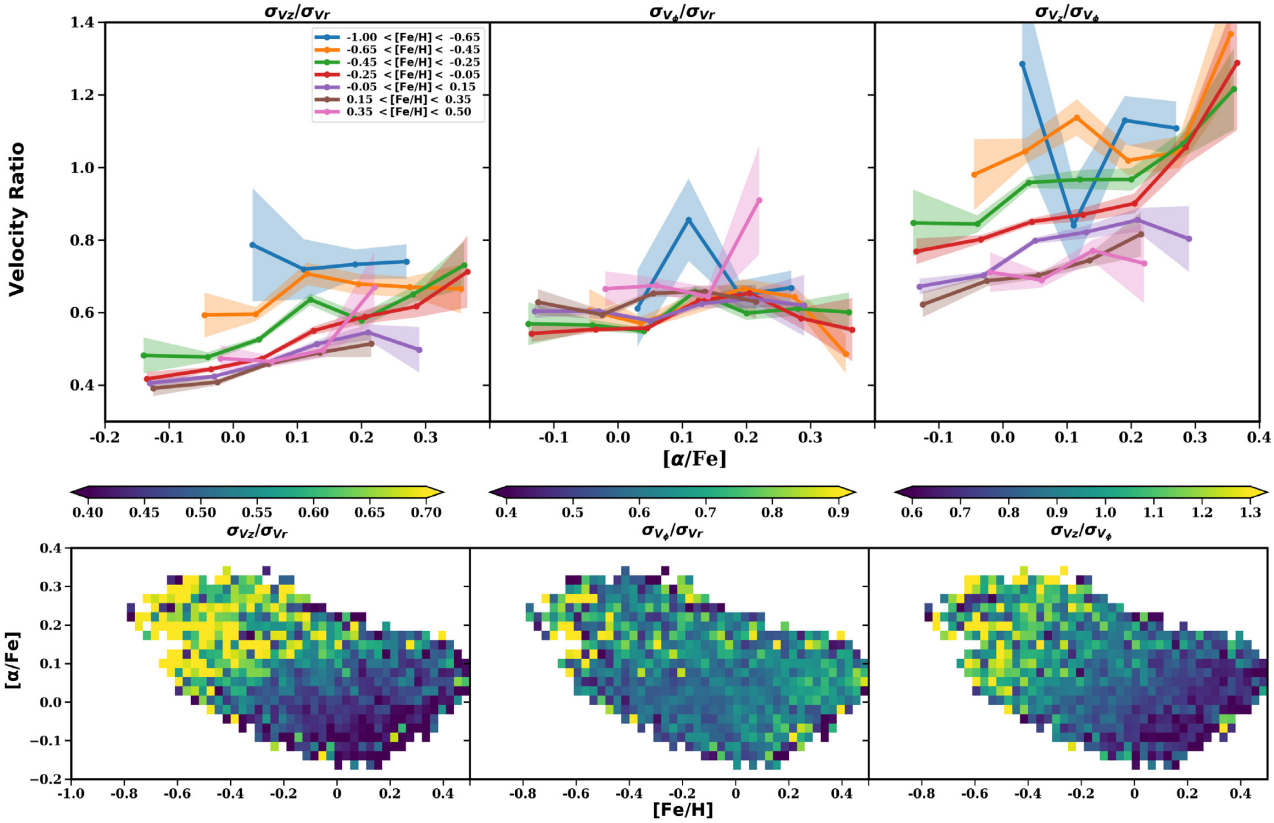


**Figure 6.** Top: The ratio of the velocity dispersions compared as a function of [$\alpha$/Fe] and colour coded by [Fe/H]. Each bin contains a minimum of 20 stars. Bottom: Similar to above, but in the [$\alpha$/Fe] versus [Fe/H] plane, colour coded by the velocity dispersion ratio. Each bin has a minimum of 10 stars. Note that the ratio of rotational velocity dispersion to radial velocity dispersion is roughly constant, so there is little structure in the middle bottom panel.

of stars can be used to try to disentangle the dynamical mechanisms responsible for causing stars of a range of birth radii to be observed in the solar neighbourhood, in particular the eccentricity. The eccentricity distribution as a function of [$\alpha$/Fe] and [Fe/H] as shown in Fig. 9. For low-[$\alpha$/Fe] populations ([$\alpha$/Fe] $< 0.1$ dex), the median eccentricity is relatively invariant with metallicity, with perhaps a slight increase of median eccentricity of 0.1 at the lowest [$\alpha$/Fe] abundances to $\sim$0.15 at intermediate [$\alpha$/Fe]. However, after this point the median eccentricities begin to increase with [$\alpha$/Fe] for all populations, but the increase is steepest for the more metal-poor stars, up to a maximum of $\sim$0.35 for the more metal-poor high-[$\alpha$/Fe] populations. These stars are on fairly elliptical orbits with large variation in radius due to epicyclic motion, and spend most of their time outside of the solar neighbourhood.

The exact origin of stars is difficult to constrain because of mixing processes such as migration, which have the ability to move a star several kpc while preserving other orbital properties such as eccentricity. Only the most metal-rich (Fe/H] $> 0.1$) stellar populations can be definitively argued to have an origin outside of the solar location. Because of their metallicities, these stars are likely to have been formed in the inner disc, where metallicities are much higher than the local ISM metallicity. As shown in the right-hand panel of Fig. 10, these stars have what appears to be a bimodal distribution in eccentricity, with the dominant peak at low eccentricity ($\sim$0.1) and a second population with eccentricities centred about $e \sim 0.2$. More than 70 per cent of these stars have eccentricities less than 0.2. More than half (55 per cent) are on very circular orbits with $e < 0.15$, and have relatively small epicyclic motions. For stars with [Fe/H] $> 0.3$, the ratio drops slightly to 62 per cent with $e < 0.2$ and 46 per cent with $e < 0.15$. The overall fraction has decreased, but still a majority are on relatively circular orbits.

The required eccentricity for a star of a given metallicity to reach the solar neighbourhood via blurring can also be estimated in a Keplerian potential using several crude assumptions. First, we assume a metallicity gradient that has not evolved in time. The metallicity gradient of young stellar populations has been measured to be $-0.07$ dex kpc$^{-1}$ (e.g. Luck et al. 2011; Anders et al. 2017). We can get a rough estimate of the birth radius of a star given its observed metallicity, the gradient of $-0.07$ dex kpc$^{-1}$, and assuming the local ISM ($R = 8.2$ kpc) is currently solar. This, combined with an assumption that the apogalacticon of the star's orbit is its present-day location in the solar neighbourhood (an assumption that heavily favours blurring), allows us to estimate the eccentricity required to reach the solar neighbourhood as shown below:

$$e(\mathrm{Fe/H}) = \frac{R_{\mathrm{ap}}}{R_g([\mathrm{Fe/H}])} - 1. \quad (7)$$

Here $R_{\mathrm{ap}}$ is the apogalacticon of the orbit and assumed to be its present-day $R$, and $R_g$ is the guiding radius, assumed to be its birth radius derived from its metallicity. As all of the stars in our sample are within 500 pc of the Sun and given our previous assumptions, the $R_{\mathrm{ap}}$ of stars in our sample lie between 7.7 and 8.7 kpc, while the required guiding radius can be as small as one kpc for a star with [Fe/H] $= 0.5$. This relation is shown as the dashed line in the right-hand panel of Fig. 10, along with the eccentricity distribution as a function of [Fe/H] for our observed metal-rich sample. Stars lying to the left/above the line are able to reach the solar neighbourhood



Downloaded from https://academic.oup.com/mnras/article/493/2/2952/5733167 by piyush.suneet@gmail.com on 24 July 2021

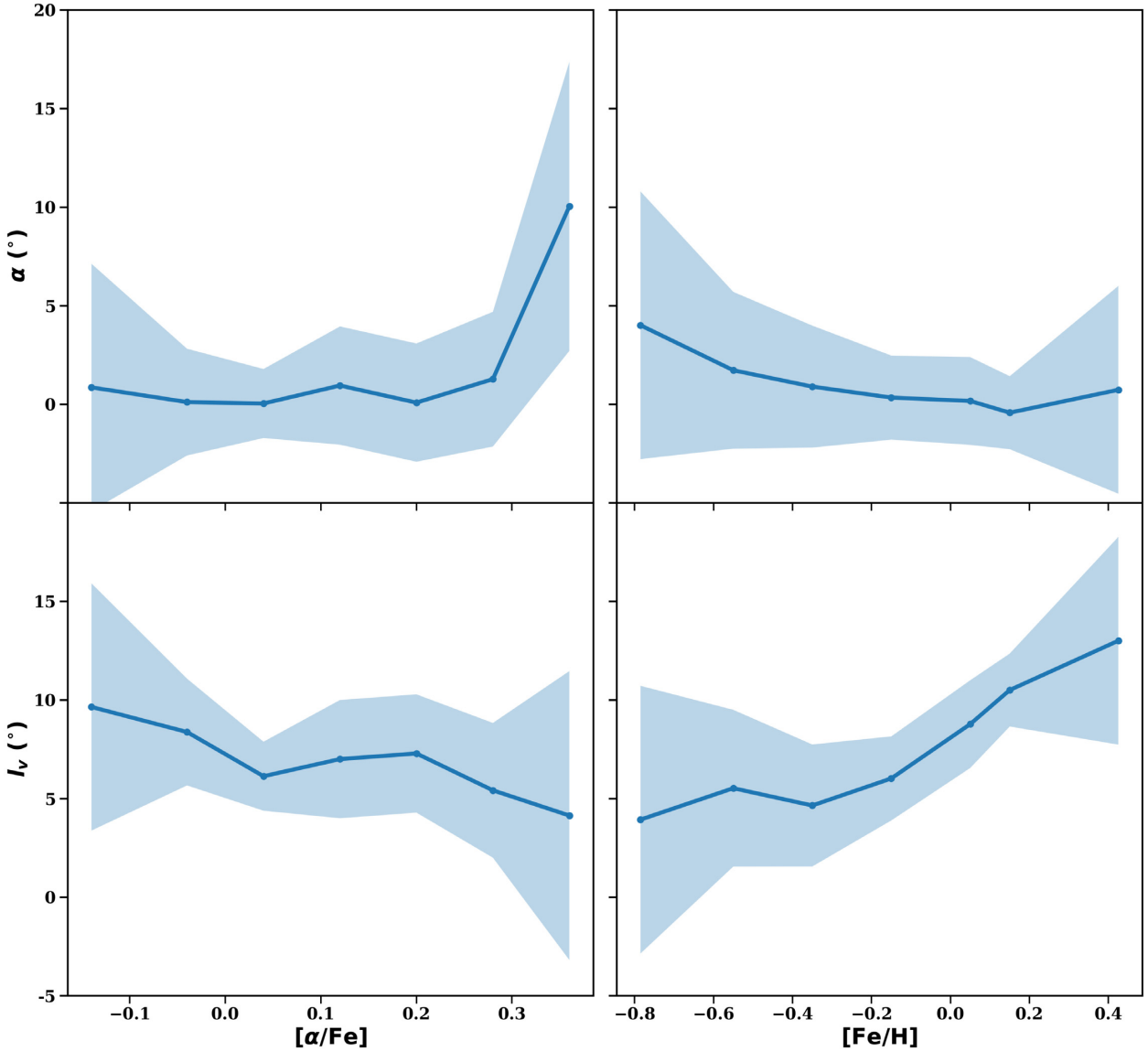


**Figure 7.** Top left: The tilt angle as a function of [$\alpha$/Fe]. Top right: The tilt angle as a function of [Fe/H]. Bottom left: The vertex deviation as a function of [$\alpha$/Fe]. Bottom right: The vertex deviation as a function of [Fe/H].

through blurring, while stars to the right/below the line cannot be explained by blurring alone given their measured [Fe/H] and $e$. More than 80 per cent of the metal-rich sample lie below the line. This finding has important implications for the roles migration and blurring play on Galactic evolution.

## 4 DISCUSSION

The smooth variation of velocity dispersion as a function of chemistry is a surprising result, given the incredible amount of substructure in velocity space found locally (e.g. Antoja et al. 2018; Hunt et al. 2018; Quillen et al. 2018; Trick et al. 2018; Bland-Hawthorn et al. 2019). In particular, for the vertical velocity dispersion, no metallicity bin (aside from the most metal-rich stellar populations) crosses another metallicity bin in velocity dispersion as a function of [$\alpha$/Fe]. This likely implies that the stars belonging to each particular substructure in velocity space has a similar Galactic origin, as the velocity dispersion would likely show larger variations with chemistry if the various velocity substructures had a variety of different Galactic origins. The smooth variation of velocity dispersion with chemistry is similar to that observed using SEGUE observations (Bovy et al. 2012), with the velocity dispersion and scale heights for different mono-abundance populations varying gradually with chemistry, or to that found with HARPS data which show the velocity dispersion smoothly varying with age (Haywood et al. 2013; Hayden et al. 2017).

Interestingly, the velocity dispersion at a given [$\alpha$/Fe] abundance is narrow for the thin disc, $<10$ km s$^{-1}$, while for the higher [$\alpha$/Fe] populations there is much larger spread at a given [$\alpha$/Fe] as a function of metallicity, with the metal-rich populations having much lower dispersions than metal-poor. It is known that there is a tight age–$\alpha$-metallicity relation for the thick disc stars (e.g. Haywood et al. 2013; Hayden et al. 2017), with an age spread of $\sim$2–3 Gyr for high-[$\alpha$/Fe] populations. This means that metal-rich stars are likely younger than metal-poor stars at high-[$\alpha$/Fe] and therefore likely to have lower velocity dispersions. This is not the case for the thin disc populations, where there is a spread of ages at a given [$\alpha$/Fe] and [Fe/H]. Additionally, studies of high-redshift galaxies



Downloaded from https://academic.oup.com/mnras/article/493/2/2952/5733167 by piyush.suneet@gmail.com on 24 July 2021

**Table 3.** The tilt of the velocity ellipsoid for the GALAH sample in the solar neighbourhood.

| [α/Fe] range | $N$ | $l_v$ (deg) | $\alpha$ (deg) |
|---|---|---|---|
| $-0.2 < [\alpha/Fe] < -0.08$ | 1842 | 9.6 ± 6.5 | 0.9 ± 6.5 |
| $-0.08 < [\alpha/Fe] < 0.0$ | 14974 | 8.4 ± 2.7 | 0.1 ± 2.7 |
| $0.0 < [\alpha/Fe] < 0.08$ | 24203 | 6.1 ± 1.9 | 0.0 ± 1.9 |
| $0.08 < [\alpha/Fe] < 0.16$ | 7597 | 7.0 ± 2.9 | 0.9 ± 2.9 |
| $0.16 < [\alpha/Fe] < 0.24$ | 3047 | 7.3 ± 3.1 | 0.1 ± 3.1 |
| $0.24 < [\alpha/Fe] < 0.32$ | 1788 | 5.4 ± 3.4 | 1.3 ± 3.4 |
| $0.32 < [\alpha/Fe] < 0.4$ | 230 | 4.1 ± 7.3 | 10.0 ± 7.3 |
| [Fe/H] Range | $N$ | $l_v$ (°) | $\alpha$ (°) |
| $-1.0 < [Fe/H] < -0.65$ | 558 | 3.9 ± 6.7 | 4.0 ± 6.7 |
| $-0.65 < [Fe/H] < -0.45$ | 2311 | 5.5 ± 4.3 | 1.7 ± 4.3 |
| $-0.45 < [Fe/H] < -0.25$ | 7283 | 4.6 ± 3.1 | 0.9 ± 3.1 |
| $-0.25 < [Fe/H] < -0.05$ | 15071 | 6.0 ± 2.2 | 0.3 ± 2.2 |
| $-0.05 < [Fe/H] < 0.15$ | 18007 | 8.8 ± 2.2 | 0.2 ± 2.2 |
| $0.15 < [Fe/H] < 0.35$ | 8375 | 10.5 ± 1.8 | −0.4 ± 1.8 |
| $0.35 < [Fe/H] < 0.5$ | 1667 | 13.0 ± 5.1 | 0.7 ± 5.1 |

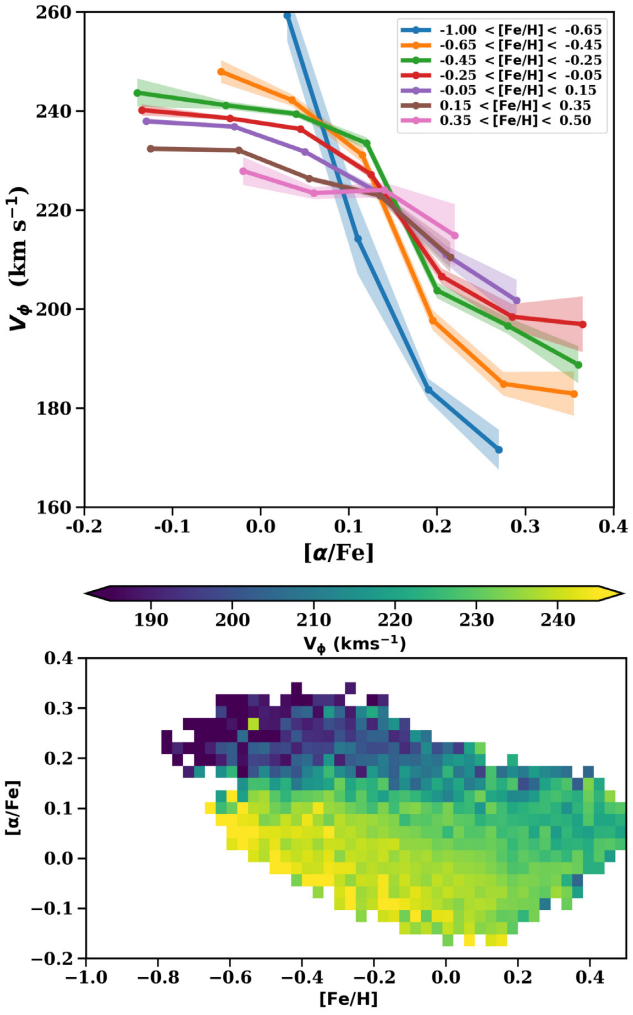


**Figure 8.** Top: The median rotational velocity a function of [α/Fe] and [Fe/H] for the GALAH solar neighbourhood sample. There is a minimum of 20 stars per bin. Bottom: The median rotational velocity in the [α/Fe] versus [Fe/H] plane. There is a minimum of 10 stars per bin. The limits of the colourbar are set to maximize contrast in each figure, there are some bins with higher (lower) rotational velocities than the upper (lower) limits.

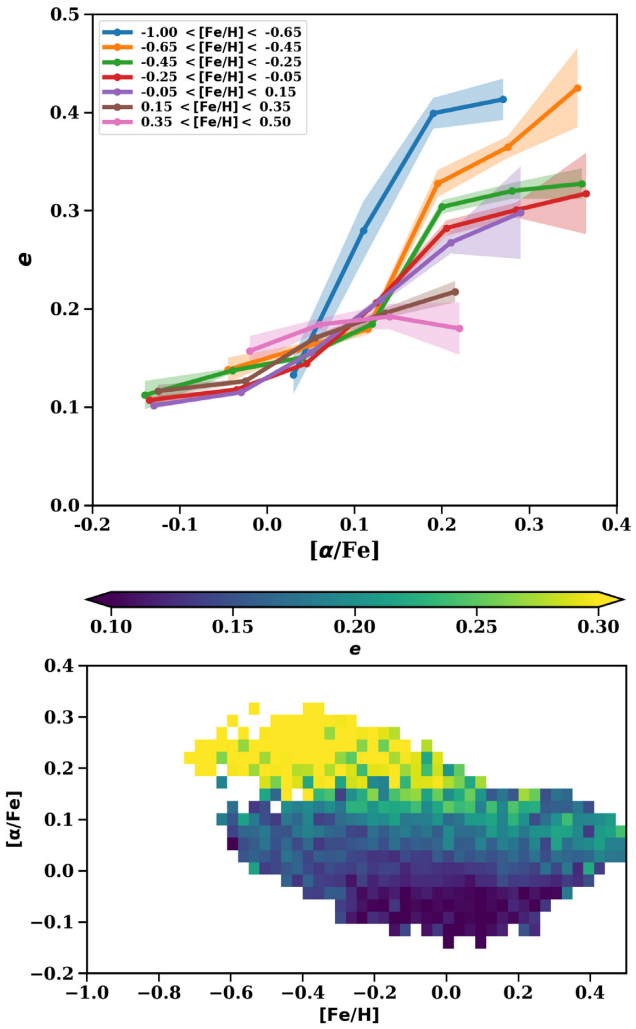


**Figure 9.** Top: The median eccentricity as a function of [α/Fe] and [Fe/H], with a minimum of 20 stars per bin. Bottom: Similar to above, but in the [α/Fe] versus [Fe/H] plane. There is a minimum of 10 stars per bin. Eccentricity increases with alpha, and for the high-[α/Fe] populations metal-rich stars have lower eccentricities than metal-poor stars with the same [α/Fe] on average. The limits of the colourbar are set to maximize contrast in each figure; there are some bins with higher (lower) eccentricities than the upper (lower) limits.

(Wisnioski et al. 2015) have found that the velocity dispersions are already high in the early universe ($z \sim 2$), and quickly settle to low-velocity dispersion thereafter, before $z \sim 1$. This matches closely our results here: metal-poor high-[α/Fe] stars are the oldest in the disc, and likely existed at a time when the disc itself was turbulent and kinematically heated. The more metal-rich high [α/Fe] are younger, and were likely born after the disc had begun to settle. The disc is also heated with time via scattering processes, but this scenario seems less likely to be able explain the large variation in velocity dispersion for the high-[α/Fe] populations. The age difference between a metal-rich and metal-poor high-[α/Fe] star is not large (∼9–10 Gyr compared to ∼11 Gyr): both populations are still old and if heating via scattering processes is the source, the difference in velocity dispersion should be small.

There has been evidence from previous spectroscopic studies that the signature of a major merger is visible in the velocity dispersion of local disc stars. Minchev et al. (2014) found this



Downloaded from https://academic.oup.com/mnras/article/493/2/2952/5733167 by piyush.suneet@gmail.com on 24 July 2021

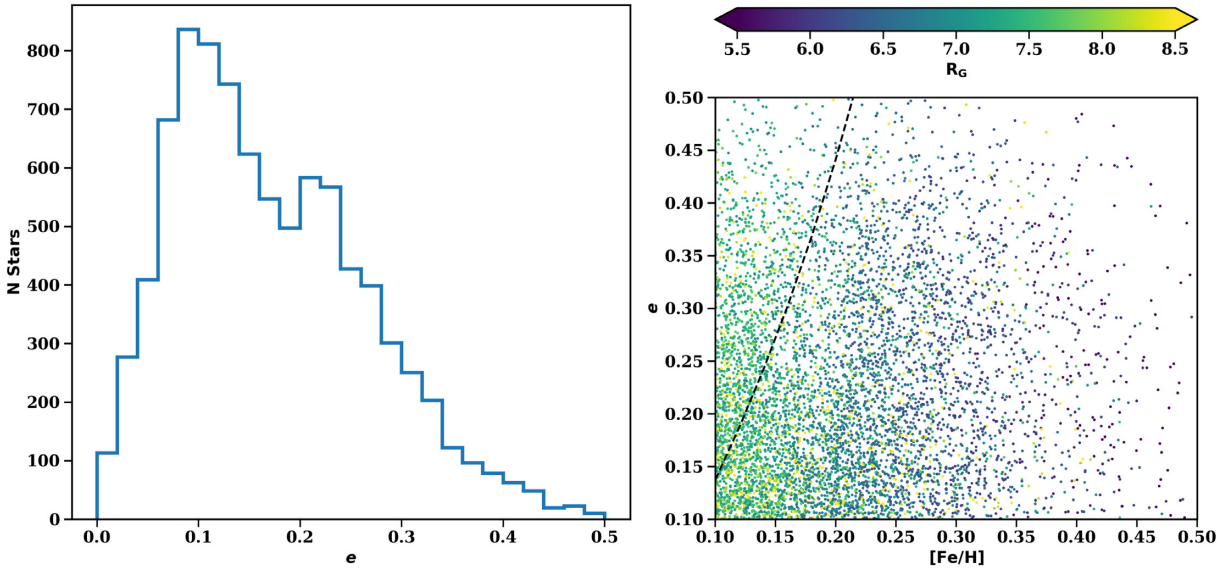


**Figure 10.** Left: The distribution of orbital eccentricities for metal-rich ([Fe/H] > 0.1 dex) stellar populations. Right: The eccentricity as a function of [Fe/H] for metal-rich stars, colour coded by the guiding radius of the orbit $R_G$. The dashed line denotes the minimum required eccentricity for a star to be observed in the solar neighbourhood, given its metallicity and a radial gradient of $-0.07$ dex kpc$^{-1}$. Stars lying to the right/below the line require migration in order to be observed in the solar neighbourhood. The limits of the colourbar are set to maximize contrast in each figure; there are some bins with higher (lower) guiding radii than the upper (lower) limits.

as a sharp decrease in the velocity dispersion for the highest [$\alpha$/Fe] populations using RAVE data. This signal was also observed in simulations from Minchev et al. (2013), which found that the dip in velocity dispersion for the highest [$\alpha$/Fe] components corresponds to enhanced migration driven by the last major merger present in the simulation. This result was less obvious in higher resolution spectroscopic studies (Guiglion et al. 2015; Hayden et al. 2018), although potentially still present within the uncertainties. However, with the advent of *Gaia* and high-precision chemistry and radial velocity measurements from GALAH, the uncertainties in both chemistry and kinematics are significantly reduced, with the velocity precision in particular an order of magnitude better compared to previous studies. With this higher precision data, we find no evidence of a significant decrease in velocity dispersion for the highest [$\alpha$/Fe] stellar populations. There appears to be a flattening in slope of the change in velocity dispersion with [$\alpha$/Fe] at high-[$\alpha$/Fe], but not the dramatic decrease as found in the RAVE observations. Similarly, a recent study by Di Matteo et al. (2019) using APOGEE observations also found no dramatic decrease in the velocity dispersion for the highest [$\alpha$/Fe] stellar populations; finding the dispersions for these stars matched those of the thick disc. The signal found in RAVE is likely the result of large uncertainties in [$\alpha$/Fe], [Fe/H], and in particular the available proper motions. This does not rule out that major mergers have had an impact on the evolutionary history of the Milky Way, merely that the signal observed in previous spectroscopic studies is unable to be reproduced with higher quality observations.

The ratio of the vertical velocity dispersion to the radial velocity dispersion provides insight into different disc heating processes. Arguments of vertical heating via giant molecular cloud scattering predict a ratio of $\sigma_{v_z}/\sigma_{v_R} = 0.62$ (Ida, Kokubo & Makino 1993; Sellwood 2008; Sellwood 2014). This is roughly the average for the more metal-poor and higher [$\alpha$/Fe] populations observed with GALAH. However, there is clearly a trend of increasing $\sigma_{v_z}/\sigma_{v_R}$ as [$\alpha$/Fe] increases. Aumer & Binney (2009) find that the $\sigma_{v_z}/\sigma_{v_R}$ is related to the age of the stellar population, as the rate of change of the vertical velocity dispersion as a function of time is greater than that of the radial velocity dispersion. This results in an increase in the $\sigma_{v_z}/\sigma_{v_R}$ ratio for older stellar populations. To the extent that [$\alpha$/Fe] can be a rough proxy for age (see Haywood et al. 2013; Hayden et al. 2017), with older stellar populations having larger [$\alpha$/Fe] abundances, we find the same trends in the GALAH data. Sharma et al. (2014) determine the $\sigma_{v_z}/\sigma_{v_R}$ ratio for different stellar populations observed with RAVE using two different models for the velocity profile of the disc (a Gaussian distribution function and a Shu distribution function Shu 1969). For the thick disc, they find $\sigma_{v_z}/\sigma_{v_R} = 0.8$ using a Shu model and $\sigma_{v_z}/\sigma_{v_R} = 0.68$ for a Gaussian model, which bracket our values for the highest [$\alpha$/Fe] stellar populations (classical thick disc stars) of $\sigma_{v_z}/\sigma_{v_R} = 0.7$. A direct comparison to their thin disc is somewhat difficult, as their model provides an estimate of $\sigma_z/\sigma_R$ as a function of time. For young-intermediate age thin disc populations (~3 Gyr), they find $\sigma_{v_z}/\sigma_{v_R} = 0.44$, gradually increasing to 0.65 for the oldest thin disc stars (~10 Gyr). Our estimations for the chemical thin disc ([$\alpha$/Fe] < 0.15 dex) fall inside this range, and perhaps hint that our lower [$\alpha$/Fe] sample is made up of fairly young stars in general (~3–5 Gyr).

We find our results of the vertex deviation and tilt angle in general agreement with recent studies near the solar position. Smith, Whiteoak & Evans (2012) found both vertex deviation and tilt angle measurements of ~10 deg using SDSS observations, with significant uncertainties in both measurements. We find a similar value for the vertex deviation, but a value more consistent with 0 for the tilt angle. Tian et al. (2015) measure a tilt angle of 0 deg, and that the vertex deviation was small for stars in the plane (0 deg) and increased as $z$ increased. This matches our results, except that we find that the vertex deviation decreases for high-dispersion populations (i.e. metal-poor or high-[$\alpha$/Fe]) and is largest for the most metal-rich stars close to the plane. Our results are in good agreement with those of Yu & Liu (2018), who find the tilt angle

Downloaded from https://academic.oup.com/mnras/article/493/2/2952/5733167 by piyush.suneet@gmail.com on 24 July 2021

consistent with zero, as well as the vertex deviation being around ∼10 deg for metal-rich stars and closer to zero for metal-poor stars observed with LAMOST.

With the advent of *Gaia* astrometry, more recent studies have been able to place additional constraints on the local velocity dispersion. Anguiano et al. (2018) measured the velocity dispersion of the local disc using a sample of high-resolution spectra and *Gaia* DR1 astrometry and found that $\sigma_{v_\phi}/\sigma_{v_R}$ is 0.67 and 0.7 for the thin and thick discs, respectively. This is in agreement with our estimates. They also find that the $\sigma_{v_z}/\sigma_{v_R}$ is 0.64 and 0.66, for the thin and thick discs, respectively, which while not dramatically different from our estimates, does not show the trend of increasing vertical velocity dispersion relative to radial velocity dispersion with [$\alpha$/Fe] as observed with GALAH. Using APOGEE DR14 and *Gaia* DR2, Mackereth et al. (2019) found that the ratio of the vertical velocity dispersion to radial velocity dispersion showed large differences for thin and thick disc populations. They find that younger (lower [$\alpha$/Fe]) populations have a large spread in this ratio, driven by guiding radius and age. For their sample in the solar neighbourhood, they find that the younger populations $\sigma_{v_z}/\sigma_{v_R}$ varies between 0.4 and 0.6 as age increases, which agrees well with our measurements for lower-[$\alpha$/Fe] populations that show similar variation between 0.4 and 0.6 as [$\alpha$/Fe] increases between −0.1 and 0.1 dex. For older (higher [$\alpha$/Fe]) populations, they find this ratio is roughly constant between 0.6 and 0.7. We find similar values for our high-[$\alpha$/Fe] populations, but a constant velocity ratio for high-[$\alpha$/Fe] populations is less obvious in our results, and our errors are large due to relatively low numbers of stars at these high-[$\alpha$/Fe] abundances. For the thick disc [Fe/H], bins where we have the most stars ($-0.65 <$ [Fe/H] $< -0.45$), we observe a flat trend for the high-[$\alpha$/Fe] populations, but at other metallicities for high-[$\alpha$/Fe] populations, we measure an increase in the ratio of the vertical velocity dispersion compared to the radial velocity dispersion. Similarly, Yu & Liu (2018) measured the age–velocity relation using LAMOST observations. We find our results in good agreements with these authors, both in the magnitude of the velocity dispersions and in the ratios. They find that the ratio of tangential to radial velocity is roughly constant at ∼0.6, similar to what we measure with GALAH observations. They find that the ratio between the vertical velocity dispersion and the tangential and radial velocity dispersion is a function of age, with $\sigma_{v_z}$ over $\sigma_{v_r}$ varying from ∼0.4 for the youngest stellar populations to ∼0.7 for older stellar populations, matching closely our results for low- and high-[$\alpha$/Fe] populations, respectively. They also find a flattening in the velocity ratio for the oldest populations.

The distribution of rotational velocities as a function of chemistry agree well with those of previous studies of the chemically selected thin and thick disc (e.g. Spagna et al. 2010; Lee et al. 2011; Recio-Blanco et al. 2014; Kordopatis et al. 2017). These authors find that the rotational velocity for the chemical thick disc increases as metallicity increases. Conversely, for the chemical thin disc, they find that rotational velocity decreases as metallicity increases. As the radial velocity dispersion is quite large for high-[$\alpha$/Fe] stars, these populations experience significant radial epicyclic motion that results in lower rotational velocities as these stars move outwards. As the radial velocity dispersion is smaller for the more metal-rich high-[$\alpha$/Fe] populations, this translates to smaller radial epicyclic motion and larger rotational velocities. The eccentricity distribution for the high-[$\alpha$/Fe] populations also mirror this result: as metallicity increases for the thick disc populations, eccentricity decreases. Dierickx et al. (2010) found that the median eccentricity for the metal-poor thick disc was ∼0.4–0.5, and that the median eccentricity of the thick disc decreased as metallicity increased, approaching that of the thin disc for the most metal-rich ([Fe/H] $> -0.2$) populations, in agreement with our results that show a clear trend of decreasing eccentricity with metallicity in the high-alpha populations. Similarly, Liu & van de Ven (2012) measured the vertical velocity dispersion and median eccentricities as a function of chemistry using observations taken from SEGUE. They find that the median eccentricity is low for low-[$\alpha$/Fe] stellar populations ([$\alpha$/Fe] ∼ 0.1–0.2) and that the median eccentricity is high for the high-[$\alpha$/Fe] thick disc populations at $e \sim 0.4$, in excellent agreement with the results presented here. They also find that the vertical velocity dispersion increases from ∼10 km s$^{-1}$ for the most metal-rich solar-[$\alpha$/Fe] populations to ∼50–60 km s$^{-1}$ for the metal-poor high-[$\alpha$/Fe] populations. Additionally, they report that the velocity dispersion is slightly higher for the metal-poor thin disc compared to the more metal-rich stars at the same [$\alpha$/Fe], similar to the results obtained in our analysis.

The trends observed in the high-[$\alpha$/Fe] populations reverse for stellar populations with solar-[$\alpha$/Fe] abundances, in which the more metal-poor stars have larger radial velocity dispersions than more metal-rich stars, and higher rotational velocities. This is likely a reflection that these more metal-poor stars have guiding radii in the outer Galaxy and, for the same conservation of angular momentum arguments above, rotate faster as they move inwards. For lower-[$\alpha$/Fe] populations, stars originating from the outer disc generally have higher rotational velocities and lower metallicities than local populations, while stars originating in the inner disc generally have higher metallicities and lower rotational velocities than local populations. The conservation of angular momentum combined with the radial gradient of the disc nicely explains the smooth trends of rotational velocity with chemistry for populations that are [$\alpha$/Fe] poor. The difference in velocity between the solar-[$\alpha$/Fe] stars is relatively minor, especially compared to the higher [$\alpha$/Fe] stellar populations that have significantly lower rotational velocities in general. These high-[$\alpha$/Fe] populations have low rotational velocities and high eccentricities, which results in large epicyclic motions and points to blurring as the likely mechanism of radial mixing that caused these stars to be observed in the solar neighbourhood. However, blurring alone may not be able to explain the presence of [$\alpha$/Fe]-poor populations in the solar neighbourhood.

The fraction of stars that reach the solar neighbourhood via blurring or migration is a topic of much debate and the relative importance of these mixing processes is critical to understanding the evolutionary history of the Galaxy. The orbital properties of stars can be used to disentangle which processes dominate in the solar neighbourhood, particularly the eccentricity distribution of the most metal-rich stars observed in the solar neighbourhood. These stars must have formed in the inner Galaxy because of their metallicity, but do not have a dramatically different rotational velocity than more metal-poor populations at solar-[$\alpha$/Fe] abundances, implying that their guiding radii are relatively close to the solar neighbourhood. This is also reflected in the eccentricity distribution of the solar-[$\alpha$/Fe] populations. The majority of the most metal-rich stars in the solar neighbourhood have $e < 0.2$. This is similar to results from Kordopatis et al. (2015) and Hayden et al. (2018), who also found that many of the most metal-rich stars in the solar neighbourhood are on fairly circular orbits. For a star with $e = 0.2$ and apogalacticon in the solar neighbourhood, the guiding radius is 6.67 kpc and the deviation from this guiding radius is only ∼1.33 kpc. This means the eccentricity must be quite high for a very metal-rich star coming from the inner Galaxy to reach the solar neighbourhood. More than 70 per cent of the stars have eccentricities $e < 0.2$, implying

Downloaded from https://academic.oup.com/mnras/article/493/2/2952/5733167 by piyush.suneet@gmail.com on 24 July 2021

their deviation from their guiding radius is <1 kpc. While there are several significant assumptions required to generate the relation shown by the dashed line in Fig. 10, it clearly demonstrates that blurring is insufficient to explain the presence of the majority of these metal-rich stars in the solar neighbourhood. Even with the simple assumptions made here, it is almost impossible for stars with [Fe/H] > 0.3 to reach the solar neighbourhood via blurring, as the orbit must be hyperbolic given their very high metallicities and the observed radial gradient of $-0.07$ dex kpc$^{-1}$. For these stars to reach the solar neighbourhood, significant angular momentum transfer (migration) must take place. Previous studies have argued that observations of the solar neighbourhood can be explained by blurring alone (e.g. Haywood et al. 2013), but our results here are at odds with that interpretation. More detailed modelling, such as the approaches taken by Minchev et al. (2018) and Feltzing, Bowers & Agertz (2020), used in conjunction with samples with accurate age determinations are required to accurately pin down the fraction of likely migrators as a function of chemistry.

It is important to note that different radial mixing processes are not mutually exclusive. A star that migrates can subsequently be heated; while a star that has had its orbit heated can migrate, particularly if that star has small vertical motion as the efficiency of migration from non-axisymmetric structure is largest for stars in the plane (Solway, Sellwood & Schönrich 2012; Vera-Ciro, D'Onghia & Navarro 2016; Daniel & Wyse 2018). The fact that the overwhelming majority of the most metal-rich stars have eccentricities incompatible with blurring alone to reach the solar neighbourhood shows that this process is a necessary component in realistic models of the chemodynamic evolution of the Galaxy. Both blurring and churning play a role in shaping the evolution of the Milky Way.

## 5 CONCLUSION

We analysed the chemodynamic structure of the local solar volume (d < 500 pc) using 62 814 stars in GALAH DR2 in conjunction with astrometric information from *Gaia* DR2. We find that the velocity dispersion generally increases smoothly as [Fe/H] decreases or [$\alpha$/Fe] increases, with the vertical velocity dispersion in particular showing no large discontinuity or even crossing in velocity space of different stellar populations. This is in stark contrast to the U-V velocity and action planes, which show several over densities and significant substructure. There is no evidence of a downturn in velocity dispersion for the highest [$\alpha$/Fe] stellar populations as previously observed with lower quality data, which indicates previous results were likely spurious. This result highlights the power that *Gaia* and large-scale spectroscopic surveys such as GALAH bring in disentangling the structure of the disc, dramatically increasing the precision and accuracy of velocity and orbital determination compared to previous studies.

The stars that are currently in the solar neighbourhood come from a large range of birth radii. How these stars reach the solar neighbourhood hold important clues on how the Milky Way disc has evolved with time. Populations with higher [$\alpha$/Fe] abundance tend to have large vertical velocity dispersion and low rotational velocities, with large asymmetric drift, implying an origin in the inner Galaxy and blurring as the dominant radial mixing process to observe these stars in the solar neighbourhood. Conversely, for the solar-[$\alpha$/Fe] populations, lower metallicity stars have much larger rotational velocities on average than the LSR, implying a Galactic origin in the outer Galaxy. Expanding this analysis to the orbital properties for stars that have metallicities much higher than the local ISM can also shed light on to different radial mixing processes of the disc. Based on the eccentricity distribution of these metal-rich stars ([Fe/H] > 0.1 dex), we find that for the majority blurring alone is unable to explain the presence of these stars near the solar position. The majority of these stars are on fairly circular orbits and simply never reach the Galactic radii at which they formed based on their high metallicities. For these stars, churning/migration is required and therefore is the dominant radial mixing process to observe these populations in the solar neighbourhood. These observations highlight the importance that migration plays in the structure and evolution of the Milky Way, realistic models of the chemodynamic history of the Galaxy must include migration in order to adequately explain observations.

## ACKNOWLEDGEMENTS

This work has made use of data from the European Space Agency (ESA) mission *Gaia* (https://www.cosmos.esa. int/gaia), processed by the *Gaia* Data Processing and Analysis Consortium (DPAC; https://www.cosmos.esa. int/web/gaia/dpac/consortium). This work is also based on data acquired from the Australian Astronomical Telescope. We acknowledge the traditional owners of the land on which the AAT stands, the Gamilaraay people, and pay our respects to elders past and present. This research was supported by the Australian Research Council Centre of Excellence for All Sky Astrophysics in 3 Dimensions (ASTRO 3D), through project number CE170100013.

In addition to ASTRO3D, MRH received support from ARC DP grant no. DP160103747. TZ acknowledges financial support of the Slovenian Research Agency (research core funding no. P1-0188). JBH is supported by an Australian Laureate Fellowship from the ARC. SLM acknowledges support from the Australian Research Council through grant no. DP180101791.

## REFERENCES

Anders F. et al., 2014, A&A, 564, A115
Anders F. et al., 2017, A&A, 600, A70
Anguiano B., Majewski S. R., Freeman K. C., Mitschang A. W., Smith M. C., 2018, MNRAS, 474, 854
Antoja T. et al., 2018, Nature, 561, 360
Asplund M., Grevesse N., Sauval A. J., Scott P., 2009, ARA&A, 47, 481
Aumer M., Binney J. J., 2009, MNRAS, 397, 1286
Bailer-Jones C. A. L., 2015, PASP, 127, 994
Balser D. S., Rood R. T., Bania T. M., Anderson L. D., 2011, ApJ, 738, 27
Balser D. S., Wenger T. V., Anderson L. D., Bania T. M., 2015, ApJ, 806, 199
Bergemann M. et al., 2014, A&A, 565, A89
Bland-Hawthorn J. et al., 2019, MNRAS, 486, 1167
Bland-Hawthorn J., Gerhard O., 2016, ARA&A, 54, 529
Bovy J., 2015, ApJS, 216, 29
Bovy J., Rix H.-W., Hogg D. W., Beers T. C., Lee Y. S., Zhang L., 2012, ApJ, 755, 115
Buder S. et al., 2018, MNRAS, 478, 4513
Buder S. et al., 2019, A&A, 624, A19
Casagrande L., Schönrich R., Asplund M., Cassisi S., Ramírez I., Meléndez J., Bensby T., Feltzing S., 2011, A&A, 530, A138
Dalton G. et al., 2014, Proc. SPIE, 9147, 91470L
Daniel K. J., Wyse R. F. G., 2018, MNRAS, 476, 1561
de Jong R. S. et al., 2014, Proc. SPIE, 9147, 91470M
Deng L.-C. et al., 2012, Res. Astron. Astrophys., 12, 735
De Silva G. M. et al., 2015, MNRAS, 449, 2604
Dierickx M., Klement R., Rix H.-W., Liu C., 2010, ApJ, 725, L186



Downloaded from https://academic.oup.com/mnras/article/493/2/2952/5733167 by piyush.suneet@gmail.com on 24 July 2021

Di Matteo P., Haywood M., Lehnert M. D., Katz D., Khoperskov S., Snaith O. N., Gómez A., Robichon N., 2019, A&A, 632, A4
Feltzing S., Bowers J. B., Agertz O., 2020, MNRAS, 493, 1419
Freeman K., Bland-Hawthorn J., 2002, ARA&A, 40, 487
Gaia Collaboration et al., 2018, A&A, 616, A1
Godwin P. J., Lynden-Bell D., 1987, MNRAS, 229, 7P
Guiglion G. et al., 2015, A&A, 583, A91
Hayden M. R. et al., 2014, AJ, 147, 116
Hayden M. R. et al., 2018, A&A, 609, A79
Hayden M. R., Recio-Blanco A., de Laverny P., Mikolaitis S., Worley C. C., 2017, A&A, 608, L1
Haywood M., Di Matteo P., Lehnert M. D., Katz D., Gómez A., 2013, A&A, 560, A109
Hunt J. A. S., Hong J., Bovy J., Kawata D., Grand R. J. J., 2018, MNRAS, 481, 3794
Ida S., Kokubo E., Makino J., 1993, MNRAS, 263, 875
Kordopatis G. et al., 2015, MNRAS, 447, 3526
Kordopatis G., Wyse R. F. G., Chiappini C., Minchev I., Anders F., Santiago B., 2017, MNRAS, 467, 469
Kos J. et al., 2017, MNRAS, 464, 1259
Lee Y. S. et al., 2011, ApJ, 738, 187
Lemasle B. et al., 2013, A&A, 558, A31
Liu C., van de Ven G., 2012, MNRAS, 425, 2144
Luck R. E., Lambert D. L., 2011, AJ, 142, 136
Luck R. E., Andrievsky S. M., Kovtyukh V. V., Gieren W., Graczyk D., 2011, AJ, 142, 51
Mackereth J. T. et al., 2019, MNRAS, 489, 176
Mackereth J. T., Bovy J., 2018, PASP, 130, 114501
Majewski S. R. et al., 2017, AJ, 154, 94
Minchev I. et al., 2014, ApJ, 781, L20
Minchev I. et al., 2018, MNRAS, 481, 1645
Minchev I., Famaey B., 2010, ApJ, 722, 112
Minchev I., Famaey B., Quillen A. C., Dehnen W., Martig M., Siebert A., 2012, A&A, 548, A127
Minchev I., Chiappini C., Martig M., 2013, A&A, 558, A9
Ness M., Hogg D. W., Rix H.-W., Ho A. Y. Q., Zasowski G., 2015, ApJ, 808, 16
Nieva M.-F., Przybilla N., 2012, A&A, 539, A143
Perryman M. A. C. et al., 2001, A&A, 369, 339
Piskunov N., Valenti J. A., 2017, A&A, 597, A16
Pryor C., Meylan G., 1993, ASPC, 50, 357
Quillen A. C. et al., 2018, MNRAS, 478, 228
Recio-Blanco A. et al., 2014, A&A, 567, A5
Rix H.-W., Bovy J., 2013, A&AR, 21, 61
Schönrich R., Binney J., 2009, MNRAS, 396, 203
Schönrich R., Binney J., Dehnen W., 2010, MNRAS, 403, 1829
Sellwood J. A., 2008, ASPC, 396, 341
Sellwood J. A., 2014, Rev. Mod. Phys., 86, 1
Sellwood J. A., Binney J. J., 2002, MNRAS, 336, 785
Sharma S. et al., 2014, ApJ, 793, 51
Sharma S. et al., 2018, MNRAS, 473, 2004
Sharma S., Bland-Hawthorn J., Johnston K. V., Binney J., 2011, ApJ, 730, 3
Sheinis A. et al., 2015, JATIS, 1, 035002
Shu F. H., 1969, ApJ, 158, 505
Smith M. C., Whiteoak S. H., Evans N. W., 2012, ApJ, 746, 181
Solway M., Sellwood J. A., Schönrich R., 2012, MNRAS, 422, 1363
Spagna A., Lattanzi M. G., Re Fiorentin P., Smart R. L., 2010, A&A, 510, L4
Steinmetz M. et al., 2006, AJ, 132, 1645
Tian H.-J. et al., 2015, ApJ, 809, 145
Trick W. H., Coronado J., Rix H.-W., 2019, MNRAS, 484, 3291
Valenti J. A., Piskunov N., 1996, A&AS, 118, 595
Vera-Ciro C., D'Onghia E., Navarro J., Abadi M., 2014, ApJ, 794, 173
Vera-Ciro C., D'Onghia E., Navarro J. F., 2016, ApJ, 833, 42
Wisnioski E. et al., 2015, ApJ, 799, 209
Wittenmyer R. A. et al., 2018, AJ, 155, 84
Yanny B. et al., 2009, AJ, 137, 4377
Yu J., Liu C., 2018, MNRAS, 475, 1093
Zwitter T. et al., 2018, MNRAS, 481, 645

This paper has been typeset from a TEX/LATEX file prepared by the author.

Downloaded from https://academic.oup.com/mnras/article/493/2/2952/5733167 by piyush.suneet@gmail.com on 24 July 2021